

Structure and vibrational dynamics of the metallic glass $\text{Ca}_{70}\text{Mg}_{30}$

J. Hafner

*Institut für Theoretische Physik, Technische Universität Wien, Karlsplatz 13, A-1040 Wien, Austria**
and Cavendish Laboratory, University of Cambridge, Madingley Road, Cambridge CB3 0HE, England

(Received 14 July 1982)

The atomic structure and the vibrational dynamics are investigated for a realistic model of the metallic glass $\text{Ca}_{70}\text{Mg}_{30}$. The calculation is based on a first-principles pseudopotential treatment of the interatomic potentials and a cluster relaxation technique for the determination of the equilibrium atomic structure and density. The recursion method has been used to compute the vibrational spectra. For the first time, a quantitative comparison between theory and experiment on the dynamical properties of a metallic glass is now possible. The theory explains successfully the low-energy vibrational modes characteristic of the amorphous state and the dispersion law for propagating collective modes.

I. INTRODUCTION

A thorough understanding of the atomic structure and the vibrational dynamics on the basis of realistic interatomic forces is a prerequisite to any understanding of the thermodynamic and the transport properties of solids. The vibrational properties of crystalline solids have been investigated extensively using optical, x-ray, and neutron spectroscopy and their theoretical description has been developed to a point where *ab initio* calculations appear to be feasible for a relatively wide class of materials.¹

For insulating amorphous solids, the wealth of experimental information offered by the various techniques of optical spectroscopy has stimulated a rapid progress in the theoretical understanding of their dynamical properties as well.² The situation is quite different for amorphous metals: Optical techniques are difficult to apply to metals and only until very recently has the progress in the preparation techniques allowed for the production of the relatively large amount of material required in an inelastic neutron scattering experiment. Progress in the theoretical description has been hampered by the fact that compared to insulating amorphous solids, metallic glasses are characterized by a larger degree of quantitative disorder and consequently a more accurate knowledge of the interatomic forces is necessary. The state of the art in the physics of the dynamical properties of metallic glasses, regarding both theory^{3,4} and experiment,⁵ has been described in recent reviews. The most important results may be very briefly summarized as follows: (a) For higher energies ($\hbar\omega \geq 10$ meV), the dynamical structure factor $S(Q, \omega)$ and the frequency distribution

$g(\omega)$ of the metallic glass are closely similar to those of the polycrystalline samples obtained after crystallization. This suggests that the vibrational properties are dominated by the short-range order in this energy region and that the short-range order is similar in the glassy and the crystalline phases. (b) The most prominent differences are found in the low-energy region below about 10 meV where additional intensity in $S(Q, \omega)$ and $g(\omega)$ is found in the glassy phase which disappears upon crystallization. These soft vibrational modes contribute to the characteristic thermodynamic, elastic, and transport properties of the metallic glass. (c) The frequency spectrum of the glassy phase is broadened at the highest vibrational energies as well, showing additional intensity above the maximum frequency of the polycrystalline phase. Very recent computer experiments⁶ suggest that these high-energy excitations are due to localized modes. (d) The Q dependence of the peak positions in the inelastic part of the dynamical structure factor $S(Q, \omega)$ show well-developed dispersion bands: The energies decrease near the first and possibly also near the second peak in the static structure factor. It has been shown that these minima in the dispersion bands arise—in close analogy to the polycrystalline case—from a “diffuse—umklapp-scattering” process.⁷

Dynamical structure factors and frequency spectra have been measured for the metallic glasses $\text{Cu}_{46}\text{Zr}_{54}$ (at room temperature),^{8,9} $\text{Mg}_{70}\text{Zn}_{30}$,^{10–12} and $\text{Ca}_{70}\text{Mg}_{30}$ (at $T=6$ K and at room temperature)^{13,14}; only the frequency spectrum has been measured in $\text{Pd}_{80}\text{Si}_{20}$.¹⁵ Theoretical investigations using either the equations-of-motion method,^{16–19} the recursion technique,^{18–21} or the Mori formal-

ism¹⁴ have been presented for a number of model systems and metallic glasses. The observed features of the frequency spectra and dynamical structure factors are generally reproduced quite well by even the simplest model calculations. However, only for Mg₇₀Zn₃₀ (Refs. 10–12 and 17) and for Cu-Zr (Refs. 8, 9, and 21) is a direct comparison between theory and experiment possible. For the case of Cu-Zr it is difficult to draw any conclusions because theory and experiment refer to different concentrations and it is quite doubtful whether the modified Lennard-Jones 4-8 potentials used in the calculations are really a good approximation to the interatomic forces. From the point of view of the interatomic forces, the simple-metal alloys Ca-Mg and Mg-Zn seem to be the ideal systems to study: For the simple metals and their alloys effective inter-atomic potentials may be derived using pseudopotential theory and the accuracy and reliability of these potentials has been tested extensively by computations of the cohesive, structural, dynamic, and thermodynamic properties of the crystalline and liquid metals^{22,23} and alloys.^{24–27} Based on these pseudopotential derived forces, a theoretical investigation of the atomic structure^{28,17} and the dynamics¹⁷ of the metallic glass Mg₇₀Zn₃₀ has been performed. The calculated structure can be compared with the result of a recent elastic neutron scattering experiment²⁹ and turns out to be very realistic. The comparison of the q -dependent frequency spectra computed using the equations-of-motion method^{17,30,31} with the result of the inelastic neutron scattering experiments^{10–12} turns out to be much more difficult: In the long-wavelength limit and for wave numbers close to the first peak in the static structure factor (i.e., near the minimum in the dispersion relation), the q -dependent frequency spectra calculated by von Heimendahl are nonzero for $\omega=0$. If the spectra are converted to the dynamical structure factor by multiplying with the thermal occupation factor $[n(\omega)+1]/\omega$ (cf. Sec. III D), the problematic result of a one-phonon structure factor diverging at $\omega=0$ is obtained. The peaks in the q -dependent spectra appear at most as weak shoulders in the dynamical structure factor and a direct comparison with the clearly resolved inelastic peaks in the measured structure factor is only of limited value. A reinvestigation of the dynamical properties of amorphous Mg₇₀Zn₃₀ using the methods described below is now under way. A comparison of the results obtained using the equations-of-motion and the recursion techniques will be given in a forthcoming publication.

The main purpose of the present paper is to use the recursion technique^{32,33} for a calculation of the vibrational properties of a glassy Ca₇₀Mg₃₀ alloy.

We begin by introducing the interatomic potentials derived from the generalized pseudopotential theory. The equilibrium density and the static atomic structure are calculated by a novel variant of the cluster-relaxation technique. Based on the knowledge of the interatomic forces and of the structure, we can calculate the dynamical structure factor and the local vibrational densities of state. The results are used to investigate the dispersion law of collective short-wavelength excitations, the origin of the characteristic low-energy vibrations, the onset of localization in high-frequency vibrations, and the interrelations between vibrational dynamics and the elastic and the thermodynamic properties of the metallic glass.

II. INTERATOMIC POTENTIALS AND STATIC STRUCTURE

In any binary metallic alloy, the ground-state energy E may be written as the sum of a volume energy $E_0(V)$ and of a pair energy $E_p(V)$ expressible as a sum over central, volume-dependent pair interactions $V_{\alpha\beta}(R, V)$:

$$E(V) = E_0(V) + E_p(V), \quad (1)$$

$$E_p(V) = \frac{1}{2} \sum_{\alpha, \beta = A, B} \sum_{i(\alpha) \neq j(\beta)} \sum_{j(\beta)} V_{\alpha\beta}(|\vec{R}_i - \vec{R}_j|, V). \quad (2)$$

The sum $\sum_{i(\alpha)}$ extends over all sites occupied by α atoms. $E_0(V)$ and the effective pair potentials may be calculated within the framework of the generalized pseudopotential theory.²⁴ They are given by

$$E_0(V) = E_{FE}(V) - \frac{2}{\pi} \sum_{\alpha = A, B} c_\alpha Z_\alpha^* \int_0^\infty F_{\alpha\alpha}^N(q) dq - \sum_{\alpha, \beta = A, B} c_\alpha c_\beta \lim_{q \rightarrow 0} \frac{4\pi Z_\alpha^* Z_\beta^*}{\Omega_0 q^2} [1 - F_{\alpha\beta}^N(q)] \quad (3)$$

and

$$V_{\alpha\beta}(R) = \frac{Z_\alpha^* Z_\beta^*}{R} \frac{4}{\pi} \int_0^\infty [1 - F_{\alpha\beta}^N(q)] q^{-1} \sin(qR) dq. \quad (4)$$

The $F_{\alpha\beta}^N(q)$ are the normalized energy–wave-number characteristics describing the indirect ion–electron–ion interaction between the ions α and β whose effective valence is Z_α^*, Z_β^* (concentrations c_α, c_β). Combining this indirect interaction (which is just the attraction of one ion to the screening cloud of a second ion) with the Coulomb repulsion gives the full effective interatomic potential $V_{\alpha\beta}(R)$

[Eq. (4)]. $E_{\text{FE}}(V)$ stands for the “free-electron energy” which is composed essentially by the ground-state energy of the electron gas plus the first-order perturbation energy given by the diagonal matrix element of the non-Coulombic part of the pseudopotential. Note that while $E_{\text{FE}}(V)$ is a positive, repulsive quantity (the largest contribution being the kinetic energy of the valence electrons), $E_0(V)$ is a negative attractive potential, which makes up for the biggest part of the binding energy. For the simple case of local pseudopotentials Finnis³⁴ has shown that the non-Coulombic pseudopotential contributions to the first and third terms in Eq. (3) cancel exactly and that $E_0(V)$ reduces to

$$E_0(V) = \bar{Z}(E_{\text{eg}} - \frac{1}{2}\Omega_0 B_{\text{eg}}) + \frac{1}{2} \sum_{\alpha=A,B} c_{\alpha} V_{\alpha\alpha}^{\text{BS}}(R=0). \quad (5)$$

\bar{Z} is the average nominal valence of the alloy, and E_{eg} and B_{eg} are the ground-state energy (per electron) and the bulk modulus of the electron gas. In this equation we have introduced the explicit real space form of the indirect (or band-structure) ion-electron-ion interaction

$$V^{\text{BS}}(R) = -\frac{Z_{\alpha}^* Z_{\beta}^*}{R} \frac{4}{\pi} \int_0^{\infty} F_{\alpha\beta}^N(q) q^{-1} \sin(qR) dq \quad (6)$$

in order to emphasize the fact that the second term in Eqs. (3) and (5) is just one-half of the average electrostatic interaction between an ion and its own screening electron cloud. In summary, the ground-state energy of the alloy is made up of an electron-gas part, the intra-atomic (in the sense of the pseudopotential equal to the ion plus the screening charge) ion–valence-electron interaction, and the interatomic interaction described by $V_{\alpha\beta}(R, V)$.

In spite of complicated many-body effects,³⁵ the volume energies and pair potentials calculated from first-principles pseudopotentials can now be considered as quite accurate: Phonon frequencies calculated on this basis agree with experiment within a few percent^{22,23} and detailed calculations have shown that they are also very useful in predicting phase changes in metals³⁶ and alloys,^{24–27} and the related changes in binding energy and density. These calculations also demonstrate that the pair energy contributes at most 2–3% to the binding energy and that—as a consequence of the volume dependence of the pair potentials³⁷—it is a decreasing function of the volume. Since the electron-gas term in Eq. (5) is again rather small we see that most of the binding energy is in the electrostatic intra-atomic interaction. Both the electron-gas and the

intra-atomic terms are strongly volume dependent, but with a different sign: The dominant kinetic energy term tends to expand the system whereas the intra-atomic interaction favors compression. The resulting energy dependence of the volume energy shows a slow increase with increasing volume. Hence the zero-pressure condition at the equilibrium density is met by a compensation between a positive pressure from the pair interactions and a negative pressure from the volume forces. The volume energy and the volume dependence of the pair interactions also cause the well-known violation of the Cauchy relations in metals and alloys.

The outcome of this discussion is that the conventional cluster-relaxation concept for the calculation of the equilibrium atomic structure (and, of course, a calculation of the equilibrium structure implies a calculation of the equilibrium density) must be modified. We begin with a density lower than the supposed equilibrium density, create a suitable starting structure, define appropriate boundary conditions ensuring constant density, calculate the volume energy and the pair potentials for that density, and relax the starting structure at constant density. In the next step the relaxed cluster is homogeneously compressed, $E_0(V)$ and the pair potentials are calculated for the new density, and the additional relaxation steps necessary to bring the atoms into their equilibrium positions at the new density and under the action of the modified potentials are executed.

At constant density the relaxation algorithm is identical to the steepest-gradient technique (in the configuration space of all atomic coordinates in the cluster) described by von Heimendahl^{17,38}. The relaxation was started from a rhombic dodecahedron containing 800 atoms which was cut out of the center of Finney’s³⁹ dense random packing of hard spheres model; periodic boundary conditions were applied. The distribution of the two different kinds of atoms over the available atomic positions was assumed to be random. The distorting forces on all atoms together form a multidimensional force $\vec{F}(\vec{R}^N) = \vec{\nabla}\phi(\vec{R}^N)$, $\vec{R}^N = \{\vec{R}_1, \dots, \vec{R}_N\}$, ϕ being the configurational potential energy given by the pair energy E_p [Eq. (2)]. Following the direction of $\vec{F}(\vec{R}^N)$ by stepwise computation, each atom will move continuously, leading to a unique minimum \vec{R}_{min}^N where the gradient $\vec{\nabla}\phi(\vec{R}^N)$ vanishes. \vec{R}_{min}^N represents at least a local minimum on the hypersurface of constant potential energy in configuration space. In calculating $\vec{F}(\vec{R}^N)$ interatomic interactions over a radius of $R_{\text{max}} = 3.70R_0$ (where R_0 is the radius of a mean atomic sphere) were taken into account. This corresponds to a cutoff for the interatomic potentials at the node after the second peak in the reduced radial distribution function. On the

average each particle interacts with 54 neighbors.

For each density the volume energy, the pair energy, and the total energy are calculated for the completely relaxed cluster. The results are shown in Fig. 1 and display the expected behavior. Knowing the total energy as a function of volume, we can calculate the equilibrium density. The theoretical result for the number density, $n=0.0278 \text{ \AA}^{-3}$, compares very favorably with the experimental result⁴⁰ of $n=0.0269 \text{ \AA}^{-3}$, the difference being only $\Delta n=3.3\%$. The computed density is very close to that calculated for a hypothetical hexagonal close-packed mixed crystal $\text{Ca}_{0.70}\text{Mg}_{0.30}$, $n=0.0273 \text{ \AA}^{-3}$, but lower than the average density $n=0.0290 \text{ \AA}^{-3}$.

The technique introduced here provides a basis for an *ab initio* calculation of the elastic and the plastic properties of glassy alloys. Detailed results for glassy Ca-Mg and Mg-Zn alloys are planned to be presented elsewhere.⁴¹ In the present context our interest is limited to the question of whether the pseudopotential method allows for a correct prediction of the equilibrium density. Our result demonstrates that the prediction is very accurate indeed and we turn now to a more detailed discussion of the atomic structure.

A. Partial pair correlation functions

The partial pair correlation functions calculated for the observed density together with the interatomic potentials are shown in Figs. 2(a)–2(c). The

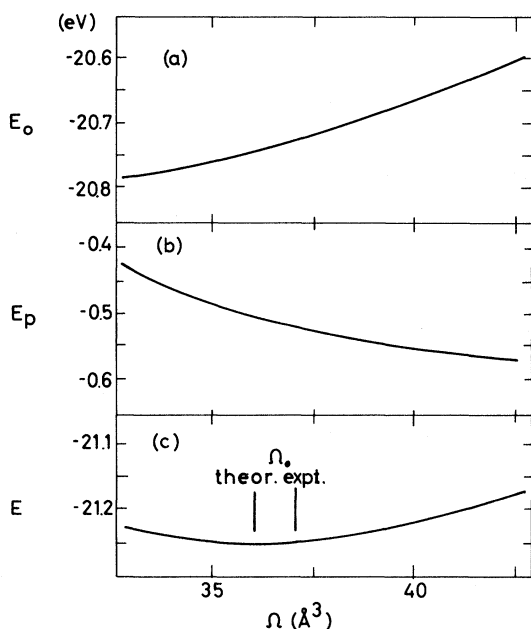


FIG. 1. Volume dependence of (a) the volume energy E_0 , (b) the pair-interaction energy E_p , and (c) the total energy E . The vertical arrows indicate the calculated and the experimental values of the equilibrium atomic volume.

results are remarkable in two respects: (i) There is a one-to-one correspondence between the minima in the interatomic potentials and the maxima in the corresponding partial pair correlation functions. This “constructive interference” ensures that the configurational energy E_p

$$E_p = 2\pi n \sum_{\alpha, \beta=A, B} c_\alpha c_\beta \int_0^\infty g_{\alpha\beta}(R) V_{\alpha\beta}(R) R^2 dR \quad (7)$$

is really a minimum for the observed structure and contributes in lowering the energy of the amorphous phase with respect to possible competing crystalline phases. The importance of this effect for the glass-forming ability has already been discussed.^{4,27,28} (ii) The pair correlation functions of the amorphous phase are very similar to those of a supercooled liquid alloy at room temperature determined by a simple thermodynamic variational technique (see Ref. 27 for details)—this shows that except for the structure in the second peak, the atomic arrangement is very liquidlike indeed.

From the partial correlation functions, the partial coordination numbers have been calculated by the method of Sadoc and Dixmier.⁴² The results, together with the mean interparticle distances are summarized in Table I. The coordination numbers may be used to estimate possible ordering. For the Cowley short-range parameter,⁴³

$$\alpha = (Z_{AA} - c_A Z) / (c_B Z), \quad (8)$$

$$Z = c_A (Z_{AA} + Z_{AB}) + c_B (Z_{BB} + Z_{BA})$$

$$= c_A Z_A + c_B Z_B,$$

we calculate $\alpha=0.15$, suggesting a small tendency to segregation. However, we must bear in mind that since the size difference is about 20%, the Cowley order parameter is not strictly applicable. The Spaepen-Cargill short-range order parameter⁴⁴

$$\eta_{AB} = Z_{AB} / Z_{AB}^* - 1, \quad (9)$$

$$Z_{AB}^* = c_B Z_A Z_B / Z$$

(Z_{AB}^* is the A - B coordination number for a random distribution of the atoms) is defined for general size ratio. With the values quoted in Table I we get $Z_{AB}=3.63$, $Z_{AB}^*=3.66$, which yields $\eta_{AB}=-0.007$. This shows that the tendency to segregation is extremely small indeed and that there is practically no chemical short-range order in amorphous $\text{Ca}_{70}\text{Mg}_{30}$.

B. Partial static structure factor and composite interference functions

The partial static structure factors calculated for the relaxed cluster are shown in Fig. 3. The results

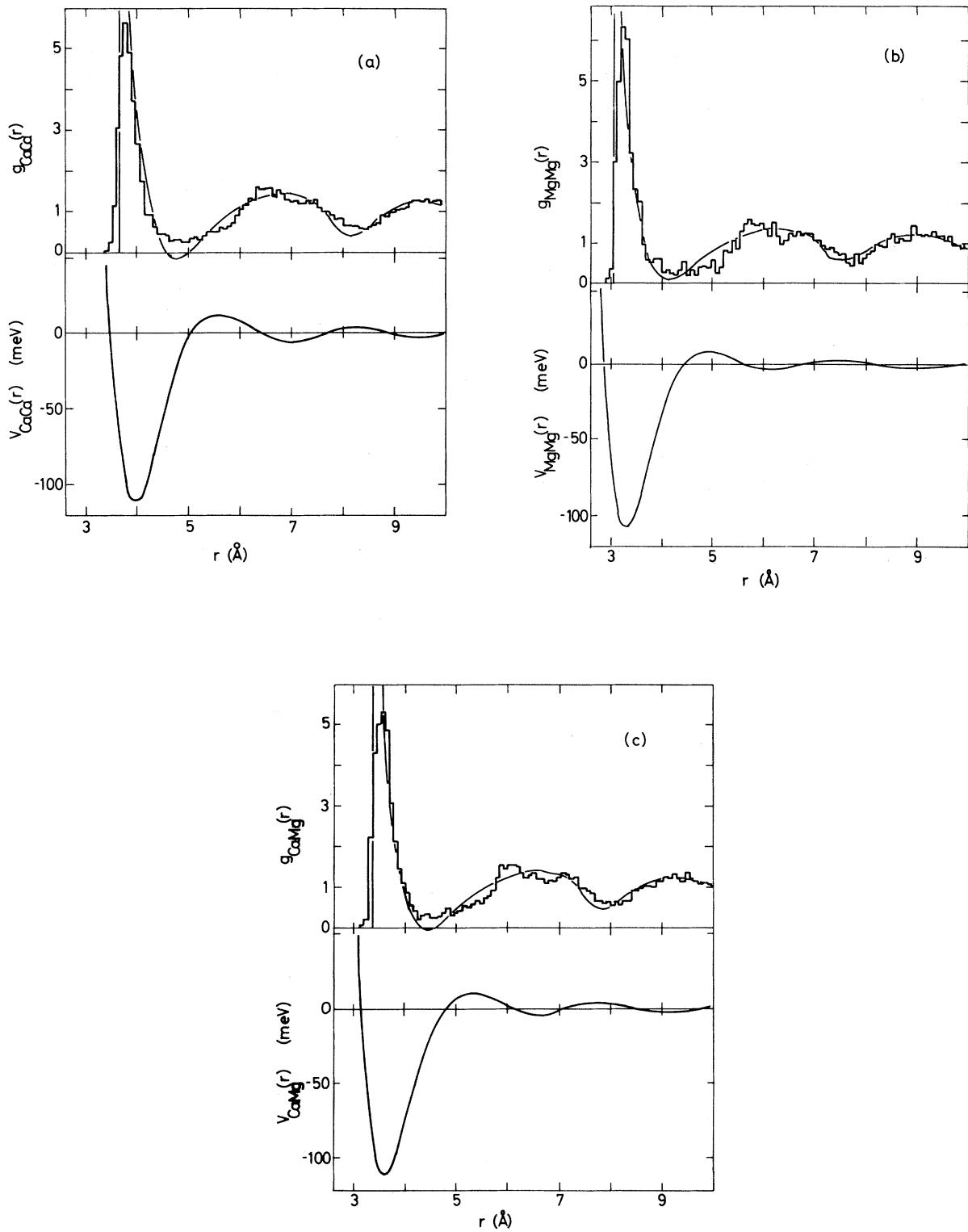


FIG. 2. Interatomic potentials $V_{\alpha\beta}(R)$ and partial pair correlation functions $g_{\alpha\beta}(R)$ for the metallic glass $\text{Ca}_{0.70}\text{Mg}_{0.30}$. The histogram describes $g_{\alpha\beta}(R)$ for the glass at $T=0$ K as calculated by the cluster-relaxation technique, the continuous line represents $g_{\alpha\beta}(R)$ for a supercooled liquid alloy at room temperature as calculated using the Gibbs-Bogoliubov thermodynamic variational technique.

TABLE I. Coordination numbers Z_{ij} and interparticle distances d_{ij} in glassy $\text{Ca}_{70}\text{Mg}_{30}$.

	Ca-Ca	Ca-Mg	Mg-Ca	Mg-Mg	Average
Z_{ij}	9.49	3.63	8.47	3.36	12.74
d_{ij} (Å)	3.82	3.52	3.52	3.22	3.74

display the same strong similarity with the static structure factors of the supercooled liquid alloy that has already been noted for the correlation functions. A scattering experiment measures a composite structure factor $S(k)$ given in terms of the partial structure factors $S_{\alpha\beta}(k)$ and the scattering form factors f_α by

$$S(k) = [c_A^2 f_A^2 S_{AA}(k) + c_B^2 f_B^2 S_{BB}(k) + 2c_A c_B f_A f_B S_{AB}(k)] / \langle f^2 \rangle, \quad (10)$$

with $\langle f^2 \rangle = c_A f_A^2 + c_B f_B^2$. Note that f_α is k dependent in the case of x-ray scattering and constant for

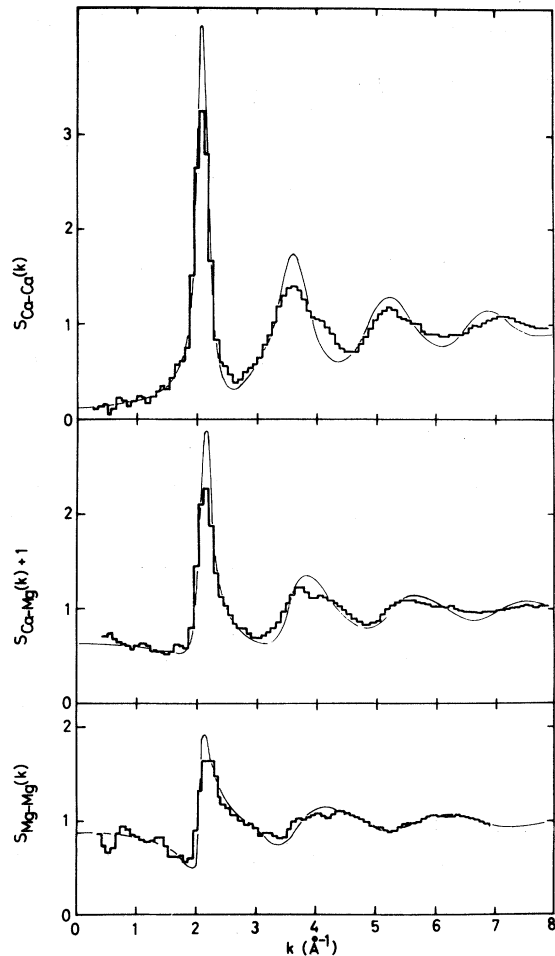


FIG. 3. Partial structure factors $S_{\alpha\beta}(k)$ for the metallic glass $\text{Ca}_{0.70}\text{Mg}_{0.30}$ (cf. Fig. 2).

neutron scattering. The neutron-weighted static structure factor is shown in Fig. 4. A static structure factor has been determined in conjunction with the inelastic neutron scattering experiment.^{13,14} Unfortunately the sample turned out to be contaminated with hydrogen and the incoherent scattering from the hydrogen atoms made a proper normalization of the measured intensity impossible. Only the positions of the first and second peak in $S(k)$ could be determined to be $Q_{p1} = 2.13 \pm 0.03 \text{ \AA}^{-1}$ and $Q_{p2} = 3.67 \pm 0.04 \text{ \AA}^{-1}$, respectively. The experimental values are practically identical with the theoretical values $Q_{p1} = 2.12 \text{ \AA}^{-1}$ and $Q_{p2} = 3.69 \text{ \AA}^{-1}$, suggesting that our structural model is very accurate. It is hoped that future experiments will verify this assumption.

C. Local structural parameters

The calculated equilibrium structure, though homogeneous on a "macroscopic" (if this denomination is allowed for an 800-atom cluster) scale, shows of course local variations in packing density, topology, and chemical order. It is highly desirable to find a set of parameters which allows the characterization of these local structural variations. A topological characterization by means of a polyhedral analyses,³⁹ interstice correlation functions,⁴⁵ or bond-angle distributions⁴⁶ proves to be very difficult. Very recently, Egami and co-workers⁴⁷ have shown that the atomic-level stresses $\sigma_i^{\alpha\beta}$ constitute a very useful set of local structural parameters which may be used to describe many physical phenomena connected with changes in the local structural arrangement.⁴⁸

In a system of interacting atoms the application of a small uniform strain will result in a change in energy. The energy change associated with the i th

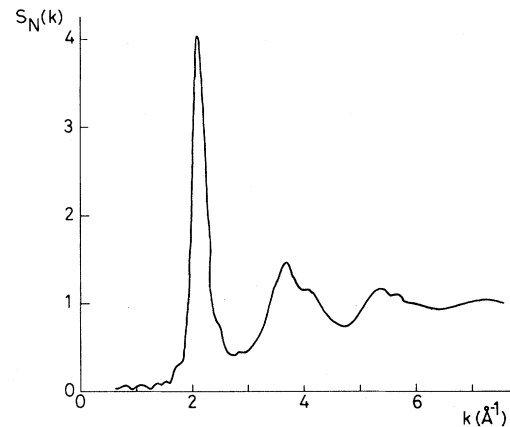


FIG. 4. Neutron-weighted total structure factor for the metallic glass $\text{Ca}_{0.70}\text{Mg}_{0.30}$.

atom is given to first order by⁴⁷

$$\Delta E_i = \Omega_i \sum_{\alpha, \beta} \sigma_i^{\alpha\beta} \epsilon^{\alpha\beta}, \quad (11)$$

where Ω_i is the local atomic volume and $\epsilon^{\alpha\beta}$ is the (α, β) component of the applied strain. The coefficients $\sigma_i^{\alpha\beta}$ define the local atomic-level stress tensor; they may be calculated from the known interatomic forces. The individual components of the stress tensor depend explicitly on the change of the coordinate system. Therefore, it is more useful to consider only the variants of the stress sensors, e.g., the local hydrostatic pressure

$$p_i = \frac{1}{3} \sum_{\alpha} \sigma_i^{\alpha\alpha} \quad (12)$$

or the average (von Mises) shear stress

$$\tau_i = \frac{1}{6} [(\sigma_i^{11} - \sigma_i^{22}) + (\sigma_i^{11} - \sigma_i^{33}) + (\sigma_i^{22} - \sigma_i^{33})^2]^{1/2}. \quad (13)$$

For a system interacting by classical pair potentials only, the expressions for the atomic-level stresses have been given by Huang⁴⁹:

$$\sigma_{i,p}^{\alpha\beta} = \frac{1}{2\Omega_i} \sum_{j \neq i} \frac{\partial V(R_{ij})}{\partial R_{ij}} \frac{R_{ij}^{\alpha} R_{ij}^{\beta}}{R_{ij}} \quad (14)$$

with $\vec{R}_{ij} = \vec{R}_i - \vec{R}_j$. In the case of an additional volume force and volume-dependent pair interactions we get a further contribution to the local hydrostatic pressure

$$p_{i,v} = \frac{\partial E_0(V)}{\partial V} + \frac{1}{2\Omega_i} \sum_{j \neq i} \frac{\partial V(R_{ij}, V)}{\partial V}, \quad (15)$$

$$p_i = \frac{\partial E_0(V)}{\partial V} + \frac{1}{6\Omega_i} \sum_{j \neq i} \left[\frac{\partial V(R_{ij}, V)}{\partial R_{ij}} R_{ij} + 3\Omega_i \frac{\partial V(R_{ij}, V)}{\partial V} \right]. \quad (16)$$

$$\phi \begin{pmatrix} i & j \\ \mu & \nu \end{pmatrix} = \frac{\partial^2}{\partial u_{i\mu} \partial u_{j\nu}} \left[\frac{1}{2} \sum_{\alpha, \beta = A, B} \sum_{k(\alpha) \neq l(\beta)} \sum_{l(\beta)} V_{\alpha\beta}(|\vec{R}_k + \vec{u}_k - \vec{R}_l - \vec{u}_l|, V) \right]. \quad (18)$$

As in the relaxation calculations, only interatomic interactions up to a maximum distance of $R_{\max} = 3.7R_0$ have been taken into account. Note that since only atomic rearrangements at constant volume are considered, the density dependence of the interatomic potentials does not show up explicitly in the dynamical problem.

Distribution histograms of the atomic-level hydrostatic pressure p_i and of the atomic-level shear stress τ_i are shown in Figs. 5 and 6. The only point in the calculation which is not really straightforward is the assignment of the local atomic volume Ω_i . Any prescription for calculating Ω_i is necessarily ambiguous to some degree. In the present calculation we have simply replaced Ω_i by the average atomic volume. This is at least consistent with our construction of the interatomic potentials which starts from the homogeneous electron gas of the mean density.

In some sense the atoms corresponding to the extreme ends of the p -distribution histogram (those with the most compressive and the most tensile stresses) and the atoms with the largest shear stresses may be considered as being located in the defect regions of the amorphous structure.⁴⁶ In the following we shall show that the atomic-level stresses are also closely related to site-dependent variations in the local vibrational density of states. A detailed discussion of atomic-level stresses, site-symmetry coefficients, and defects in realistic models of simple-metal glasses, however, will be referred to a planned publication.⁵⁰

III. VIBRATIONAL DYNAMICS

In the harmonic approximation, the Hamiltonian of our system of vibrating atoms is given by

$$H = \sum_{i,\mu} \frac{P_{i\mu}^2}{2M_i} + \frac{1}{2} \sum_{i,\mu} \sum_{j,\nu} \phi \begin{pmatrix} i & j \\ \mu & \nu \end{pmatrix} u_{i\mu} u_{j\nu}, \quad (17)$$

where the $p_{i\mu}$ and $u_{i\mu}$ are the μ -Cartesian components of the momentum and the displacement vectors of the i th atom with the equilibrium position \vec{R}_i and the mass M_i . The force-constant matrix $\phi \begin{pmatrix} i & j \\ \mu & \nu \end{pmatrix}$ is given in terms of the interatomic potentials by

The vibrational density of state projected onto an arbitrary state ψ (the vibrational spectrum of state ψ) is defined through

$$g_{\psi}(\omega) = -\frac{2\omega}{\pi} \text{Im} \langle \psi | (\omega^2 - D + i\delta)^{-1} | \psi \rangle, \quad \omega \geq 0 \quad (19)$$

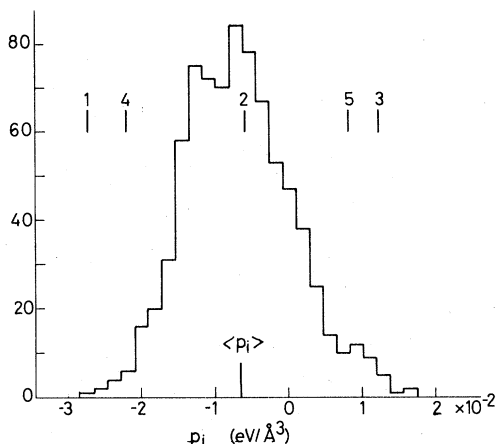


FIG. 5. Distribution histogram of the atomic-level hydrostatic pressures p_i for amorphous $\text{Ca}_{0.70}\text{Mg}_{0.30}$.

where D stands for the real-space dynamical matrix $D_{\mu\nu}^{ij} = (M_i M_j)^{-1/2} \Phi_{\mu\nu}^{ij}$. The resolvent $(\omega^2 - D + i\delta)$ in Eq. (19) is very conveniently calculated using the recursion technique of Heine *et al.*³² in the form of a continued-fraction expansion:

$$\langle \psi | (\omega^2 - D + i\delta)^{-1} | \psi \rangle = t_1, \quad (20)$$

$$t_1 = (\omega^2 + i\delta - a_1 - |b_1|^2 t_2), \quad (21a)$$

$$t_n = (\omega^2 + i\delta - a_n - |b_n|^2 t_{n+1}), \quad (21b)$$

where a_n and b_n are the (n, n) and $(n, n+1)$ elements of the tridiagonalized dynamical matrix.³² Terminating the continued fraction expansion after N sets of continued fraction coefficients (a_n, b_n) gives a discrete spectrum of N sharp spectral lines. Any analytical continuation of the continued fraction results in replacing the discrete spectrum by a smooth, continuous one. In this work we use the termination routine developed by Nex³³ which has the advantage

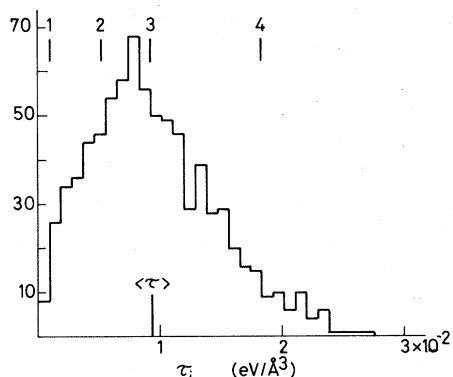


FIG. 6. Distribution histogram of the atomic-level average shear stresses (von Mises's shear stresses) τ_i for amorphous $\text{Ca}_{0.70}\text{Mg}_{0.30}$.

of producing the smoothest spectrum possible. This is important since we want to avoid any spurious structure in the spectra which might result from our using a finite cluster and periodic boundary conditions. Normally we calculate the continued fraction coefficients up to $N=15$, but the influence of the exact higher-order coefficients will be discussed briefly.

B. Local density of states

If we define $|\psi\rangle$ as the μ -polarized vibrational state of the i th atom, i.e., the

$$|\psi\rangle \text{ with } u_{j\nu} = 1, \quad j, \nu = i, \mu \quad (22)$$

$$u_{j\nu} = 0, \quad j\nu \neq i, \mu$$

the spectrum computed from Eq. (19) is the local density of states (LDOS) of the μ -polarized vibrational state of the i th atom. The LDOS on the i th atom is calculated by averaging over the possible polarizations—in our case we determined the LDOS by averaging over three polarization vectors in the directions of the coordinate axes used to describe our cluster. If, as we mentioned in the Introduction, the total vibrational density of state (TDOS) of amorphous state is smooth and has no particular distinguishing features, Figs. 7 and 8 show that this is not so for the LDOS. The shape and the center of gravity of the LDOS varies quite strongly from one

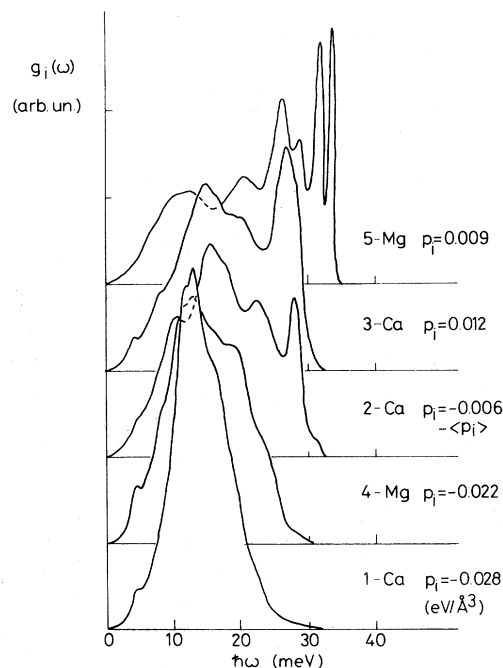


FIG. 7. Local vibrational densities of states at several atomic sites with different atomic-level pressures p_i as indicated.

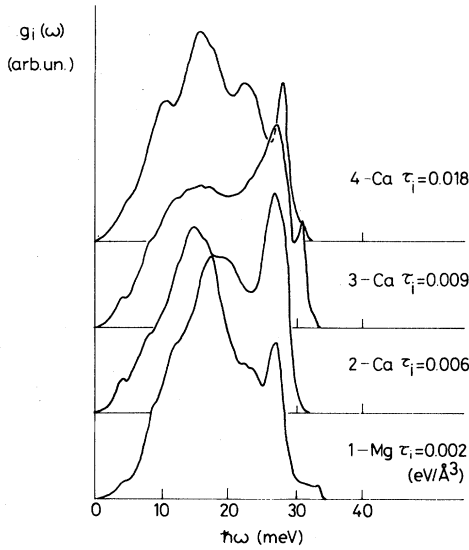


FIG. 8. Local vibrational densities of state at several atomic sites with $p_i \sim 0$ and different atomic-level shear stresses τ_i .

atomic site to another. The results assembled in Fig. 7 demonstrate that the strongest influence on the LDOS comes from the atomic-level hydrostatic pressure: For atoms under tensile stresses, the LDOS is shifted to lower frequencies, whereas for atoms under compressive stresses the higher frequencies have a larger weight. If the atom under compressive stress is of the lighter species, sharp peaks in the LDOS develop at the upper edge of the spectrum. They are strongly reminiscent of crystalline impurity modes induced by light interstitial atoms. In order to check whether the high-frequency modes centered at compressive defects are really localized modes, a study of the wave functions of the vibrational states and a calculation of the participation ratio⁵¹ will be performed.

Very recently Gompf⁵² has performed a very interesting experimental study of the influence of annealing on the vibrational spectrum of sputtered amorphous Fe-Zr alloys. He showed that the spectrum of the as-prepared alloys is strongly broadened compared to the crystalline reference spectrum; on annealing the additional low- and high-frequency excitations disappear progressively. On the other hand, Srolovitz *et al.*⁴⁷ have proposed a local microscopic mechanism of structural relaxation upon annealing which may be described essentially as a “recombination” of tensile and compressive defects. This model, combined with the present results on the LDOS appears to give an appealing explanation of Gompf’s results.

The influence of the variation of the atomic-level

shear stresses on the LDOS is by far smaller. Atoms with quite large τ_i but p_i close to zero show a LDOS which is hardly different from that of an atom in a well-relaxed region ($p_i \sim \tau_i \sim 0$).

B. Total density of states

The total vibrational spectrum may be computed in three different ways: (i) by defining $|\psi\rangle$ as

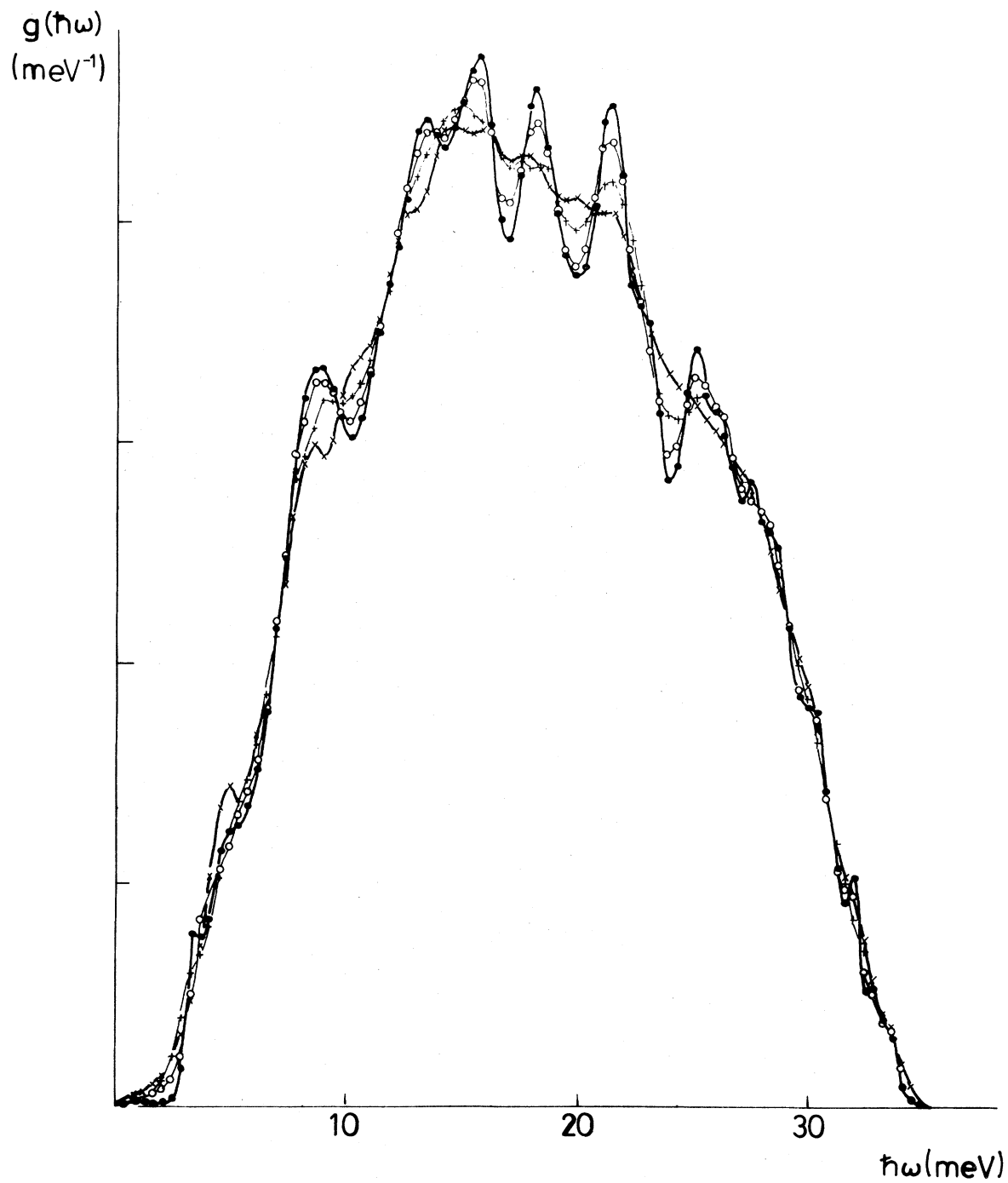
$$|\psi\rangle = \frac{1}{(3N)^{1/2}} \sum_{i,\mu} \exp(i\phi_{i\mu}), \quad (23)$$

where the $\phi_{i\mu}$ are a set of random numbers, $0 \leq \phi_{i\mu} \leq 2\pi$, and N is the number of atoms in the cluster, (ii) by averaging over a suitable set of LDOS’s, and (iii) by an incoherent sampling over the dynamical structure factor (in this case it is usual to speak of a generalized DOS, cf. Sec. III E).

The TDOS calculated according to Eqs. (19) and (23) for 12, 20, 30, and 40 recursion levels is shown in Fig. 9. It is shown that the inclusion of higher-order recursion coefficients does not alter the width and the general shape of the TDOS, but merely introduces spurious peaks into the spectrum. That these peaks are spurious is demonstrated by the fact that they appear just at the “Brillouin-zone boundary frequencies” of the Brillouin zone corresponding to the periodicity volume of the 800-atom cluster. These frequencies are easily determined from the dispersion relations to be discussed below. Hence it is reasonable to restrict the calculation of the recursion coefficients to a rather small number.

If method (ii) is to be used to compute the TDOS, one must take care to select a set of atomic sites whose average hydrostatic atomic-level stress $\langle p \rangle$ is close to zero. Any other choice would not be representative and would result in a distorted TDOS. Figure 10 demonstrates that the TDOS’s calculated by the different methods agree very well.

For our case of amorphous $\text{Ca}_{70}\text{Mg}_{30}$, comparison with experiment is complicated by the fact that the sample on which the inelastic neutron scattering experiment has been performed was contaminated by a few percent of hydrogen. Since hydrogen mainly contributes to the spectra in the region of the elastic peak and at energies above 30 or 40 meV, the results are still very instructive at energies below this critical level, the only difficulty lying in the fact that the spectra could not be properly normalized because the exact amount of the contribution stemming from H vibrations is unknown. Therefore, before comparing theory and experiment, the height of the main peak in the TDOS was matched (Fig. 11). If this is done the agreement is very good indeed, especially for low frequencies, whereas the upper edge of the frequency band seems to be slightly too high.



VIBRATIONAL SPECTRUM $\text{Ca}_{70}\text{Mg}_{30}$

-x-x- 12

-o-o- 30

... 20

-●- 40

RECURSION LEVELS

FIG. 9. Total vibrational density of states calculated with statistically distributed initial phases [Eq. (23)] and different numbers of recursion levels (-x-x-, $N=12$; -+-, $N=20$; -o-o-, $N=30$; -●-, $N=40$).

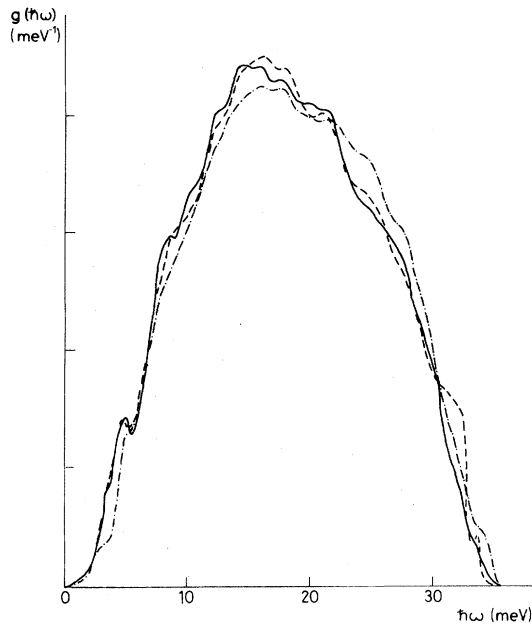


FIG. 10. Total vibrational density of states calculated with 15 recursion levels and (i) statistically distributed phases (full line), (ii) by averaging over 20 local densities of sites satisfying $\langle p_i \rangle \sim 0$ (dashed line), and (iii) generalized density of states calculated by the incoherent sampling technique over the dynamical structure factor [Eq. (31)] (dot-dashed line).

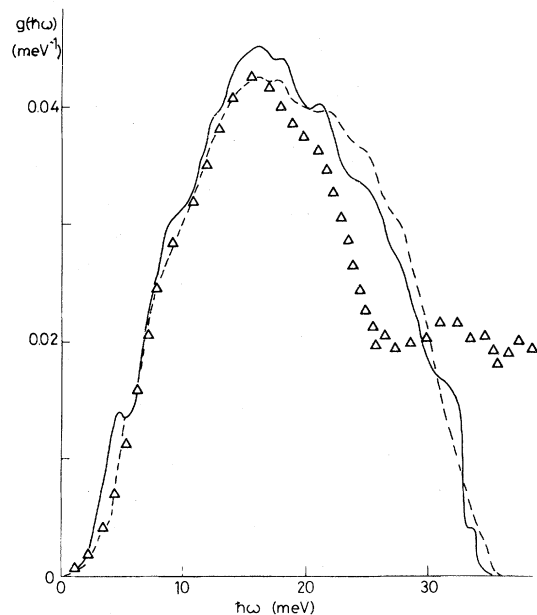


FIG. 11. Total vibrational density of states of amorphous $\text{Ca}_{70}\text{Mg}_{30}$: full line, theoretical TDOS; dashed line, generalized DOS; experiment, triangles. The experimental TDOS cannot be normalized because of incoherent scattering contributions from hydrogen impurities. Therefore, the peak height has been matched.

In crystals $g(\omega) \propto \omega^2$ for the lowest frequencies. Although the extreme-low-energy regime (the elastic part of the spectrum) is not accessible to experiment with a conventional neutron source, Suck *et al.* have argued on the basis of their experiments on amorphous Cu-Zr, Mg-Zn, and Ca-Mg alloys that this law is not obeyed in metallic glasses. Instead they showed that $g(\omega) \propto \omega^\beta$, with $\beta \sim \frac{4}{3} - \frac{3}{2}$. An investigation of this question goes to the limits of the applicability of the recursion method. Because the calculation is based on a small number of recursion levels only, there is a certain danger that the low- ω behavior of $g(\omega)$ reflects the details of the termination procedure rather than an intrinsic property of the system. The double-logarithmic plot shown in Fig. 12 however, shows good agreement between theory and experiment down to the lowest energies investigated experimentally. In the energy range $\hbar\omega = 4\text{--}8$ meV both theory and experiment point to a $\omega^{3/2}$ behavior of the TDOS.

C. Wave-number-dependent spectra

A wave-number-dependent vibrational spectrum is defined by the DOS projected onto a plane wave with wave vector \vec{k} and polarization \vec{e} ; i.e., the initial state ψ is defined by the following displacement pattern

$$|\psi\rangle = N^{-1/2} \sum_{i,\mu} e_\mu \exp(i\vec{k} \cdot \vec{R}_i), \quad (24)$$

where the e_μ are the Cartesian components of a polarization vector. Equation (24) defines the total (or density-fluctuation) spectrum $S_{NN}(k, \omega)$ via Eq. (19).

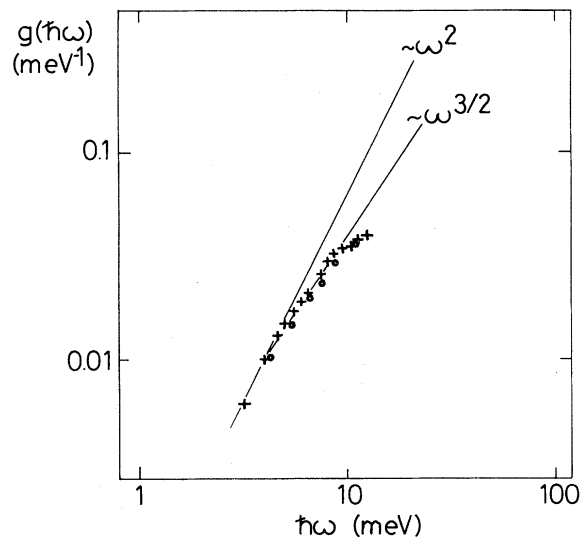


FIG. 12. Double logarithmic plot of the low-energy part of the vibrational density of state (cf. text).

A partial wave-number-dependent spectrum $S_{\alpha\alpha}(k, \omega)$, $\alpha = A, B$, is obtained if only the atoms of species α are displaced and the normalizing factor $N^{-1/2}$ is altered accordingly to $N_{\alpha}^{-1/2}$.

The wave-number-dependent spectra for longitudinal excitations are shown in Fig. 13. Note that the allowed values of k are determined by the periodic boundary conditions. All three partial spectra demonstrate the existence of well-defined longitudinal collective excitations at long wavelength, with an

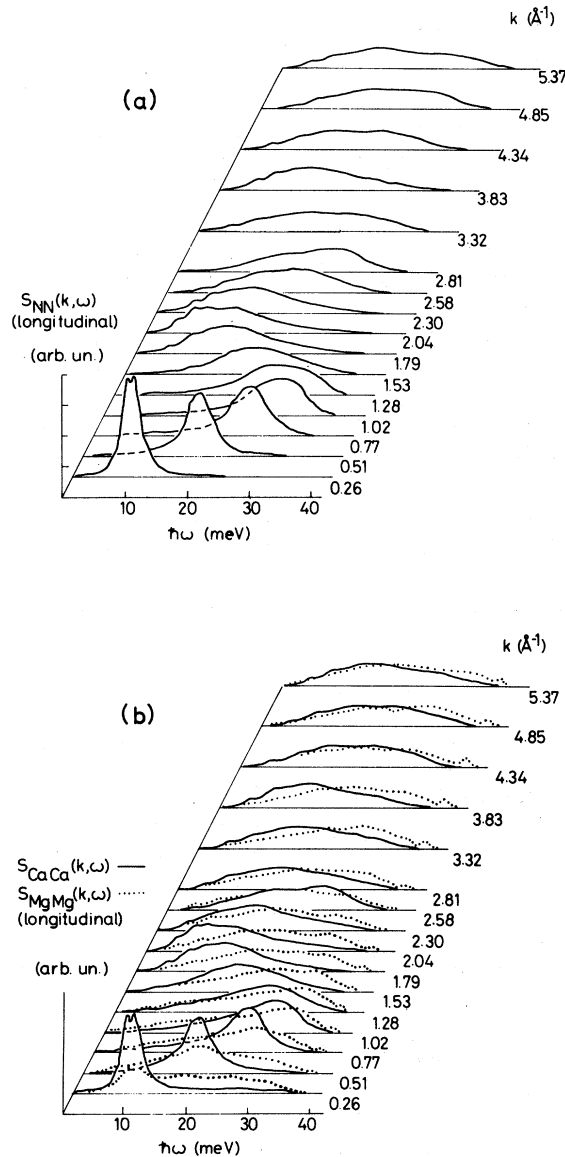


FIG. 13. Wave-number-dependent vibrational spectra $S_{\alpha\beta}(k, \omega)$ for amorphous $\text{Ca}_{70}\text{Mg}_{30}$ for longitudinal excitations. (a) Total spectrum $S_{NN}(k, \omega)$ and (b) partial spectra $S_{\text{Ca-Ca}}(k, \omega)$ and $S_{\text{Mg-Mg}}(k, \omega)$.

increasing dispersion law up to $k \sim Q_p/2$, a falling dispersion law between $Q_p/2$ and Q_p , and with the well-known “umklapp minimum” near Q_p . The partial spectra $S_{\text{Ca-Ca}}(k, \omega)$ and $S_{\text{Mg-Mg}}(k, \omega)$ are distinctly different in the elastic regime and up to about $k \sim 2Q_p$. For the longest wavelength $S_{\text{Ca-Ca}}(k, \omega)$ shows a sharply defined collective excitation, whereas $S_{\text{Mg-Mg}}(k, \omega)$ has a broad frequency band with only weak indications of a collective behavior. Up to $k \sim 2Q_p$ the Mg vibrations contribute mainly to the high-frequency part, while the Ca atoms dominate the spectrum at low frequencies. The differences in the two partial spectra are quite small beyond $k \sim 2Q_p$, where $S_{\alpha\alpha}(k, \omega) \sim S_{NN}(k, \omega) \sim g(\omega)$, indicating that the short-wavelength vibrations are predominantly incoherent.

The spectra for transverse excitations are shown in Fig. 14. Collective transverse excitations are well defined, but only for the lowest k values. As k increases, the transverse spectra are very rapidly broadened. Already for $k \sim Q_p/2$ the transverse spectrum is practically identical with the TDOS.

There have been attempts to identify “acoustic” and “optic” modes in the wave-number-dependent spectra. For large mass differences such as in transition-metal-metalloid ($\text{Fe}_x\text{B}_{1-x}$ with $M_{\text{Fe}}/M_{\text{B}} = 5.0$) or even in Mg-Zn glasses ($M_{\text{Zn}}/M_{\text{Mg}} = 2.5$) “acoustic” and “optic” are convenient, though slightly improper designations for the rather well-separated frequency bands of the heavier and the lighter atoms, respectively. In the case of Ca-Mg ($M_{\text{Ca}}/M_{\text{Mg}} = 1.5$), the frequency bands largely overlap and a separation into different modes is no longer meaningful. On the other hand, this means that the peaks in the composite (neutron-weighted) spectrum will be rather well defined even for large k 's. As we shall see in a moment, this is the reason why only in Ca-Mg can the dispersion law be determined beyond Q_p .

D. Dynamical structure factors

The coherent double-differential cross section for inelastic neutron scattering is given in terms of the dynamical structure factor $S(k, \omega)$ by

$$\frac{d^2\sigma}{d\Omega dE} = \frac{\sigma}{4\pi} \left[\frac{E}{E_0} \right]^{1/2} S(k, \omega), \quad (25)$$

where σ is the weighted bound scattering cross section, and E and E_0 are the energies of the scattered and of the incoming neutron. In the one-phonon approximation, $S(k, \omega)$ is given by [$n(\omega)$ is the Bose occupation function]

$$S(k, \omega) = -\frac{\hbar}{N} [n(\omega) + 1] \sum_{\alpha, \beta=A, B} e^{-W_\alpha(k)} e^{-W_\beta(k)} \frac{f_\alpha f_\beta}{\sqrt{M_\alpha M_\beta}} \text{Im} \langle \psi_\alpha | (\omega^2 - D + i\delta)^{-1} | \psi_\alpha \rangle, \quad (26)$$

with

$$\langle \psi_\alpha | = \frac{1}{\sqrt{N_\alpha}} \sum_{l(\alpha), \mu} e^{i\vec{k} \cdot \vec{r}_l} e_\mu k_\mu \quad (27)$$

as in Eq. (24). Thus we find that the dynamical structure factor may be expressed in terms of the wave-number-dependent spectra for longitudinal excitations as

$$\begin{aligned} S(k, \omega) &= \frac{\hbar\pi}{N} \frac{n(\omega) + 1}{2\omega} k^2 \sum_{\alpha, \beta=A, B} \frac{f_\alpha f_\beta}{\sqrt{M_\alpha M_\beta}} S_{\alpha\beta}(k, \omega) e^{-W_\alpha(k)} e^{-W_\beta(k)} \\ &= \frac{\hbar\pi}{N} \frac{n(\omega) + 1}{2\omega} k^2 [c_A(b_A^2 - b_A b_B) S_{AA}(k, \omega) + c_B(b_B^2 - b_A b_B) S_{BB}(k, \omega) + b_A b_B S_{NN}(k, \omega)], \end{aligned} \quad (28)$$

where

$$b_\alpha = e^{-W_\alpha(k)} f_\alpha M_\alpha^{-1/2}. \quad (29)$$

For any isotropic solid, the Debye-Waller factor for the atoms of species α may be calculated from the partial DOS via

$$W_\alpha(k) = \frac{\hbar^2 k^2}{M_\alpha} \int g_{\alpha\alpha}(\omega) \frac{n(\omega) + \frac{1}{2}}{\hbar\omega} d\omega. \quad (30)$$

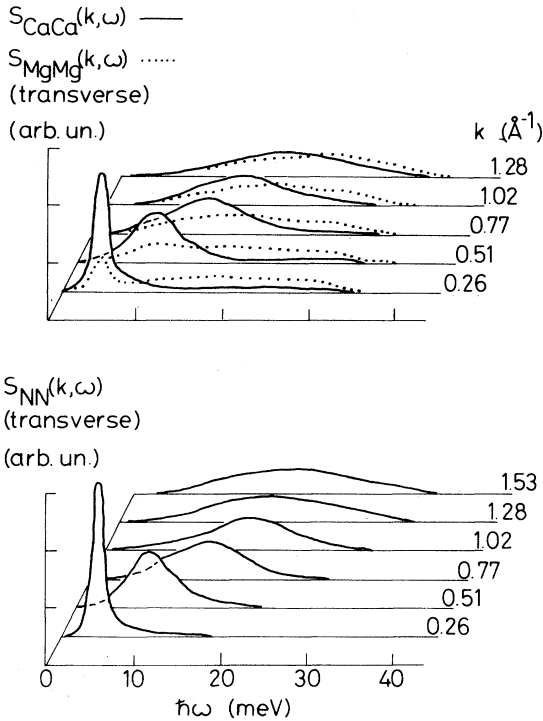


FIG. 14. Wave-number-dependent vibrational spectra for transverse excitations in amorphous $\text{Ca}_{0.70}\text{Mg}_{0.30}$.

Equation (28) has the advantage of expressing the dynamical structure factor in terms of diagonal matrix elements of the resolvent only.

In Fig. 15 the calculated dynamical structure factor is compared with experiment for $T=6$ K. Note that theory and experiment do not always refer to the same k values— $S(k, \omega)$ can be calculated only for wave numbers compatible with the periodic boundary conditions. The calculation reproduces the observed dynamical structure factors surprisingly well. In making the comparison we have to keep in mind that (i) the experimental results have not been corrected for multiple scattering and (ii) in principle the theoretical results should be folded with the resolution function of the spectrometer. Note, however, that the termination of the recursion sequence at a finite level introduces a finite resolution in the calculation result as well.

1. Temperature dependence of the normal vibrations

The experimental investigation of the dynamical structure factors of amorphous $\text{Mg}_{70}\text{Zn}_{30}$ and $\text{Ca}_{70}\text{Mg}_{30}$ at $T=6$ and 273 K has demonstrated a strong temperature dependence of the vibrational modes, especially at low excitation energies (below ~ 10 meV). The low-energy intensity is strongly enhanced and in some cases, the inelastic peak merges in the quasielastic peak. From the experiment alone, it is impossible to decide whether the observed changes reflect just the temperature-dependent variations of the Bose-occupation factor and of the Debye-Waller factor or whether they indicate anharmonic frequency shifts. In Fig. 16 we show the temperature dependence at the example of a few selected constant- k scans. It follows that the temperature dependence is perfectly reproduced by a harmonic calculation—there is no particular soften-

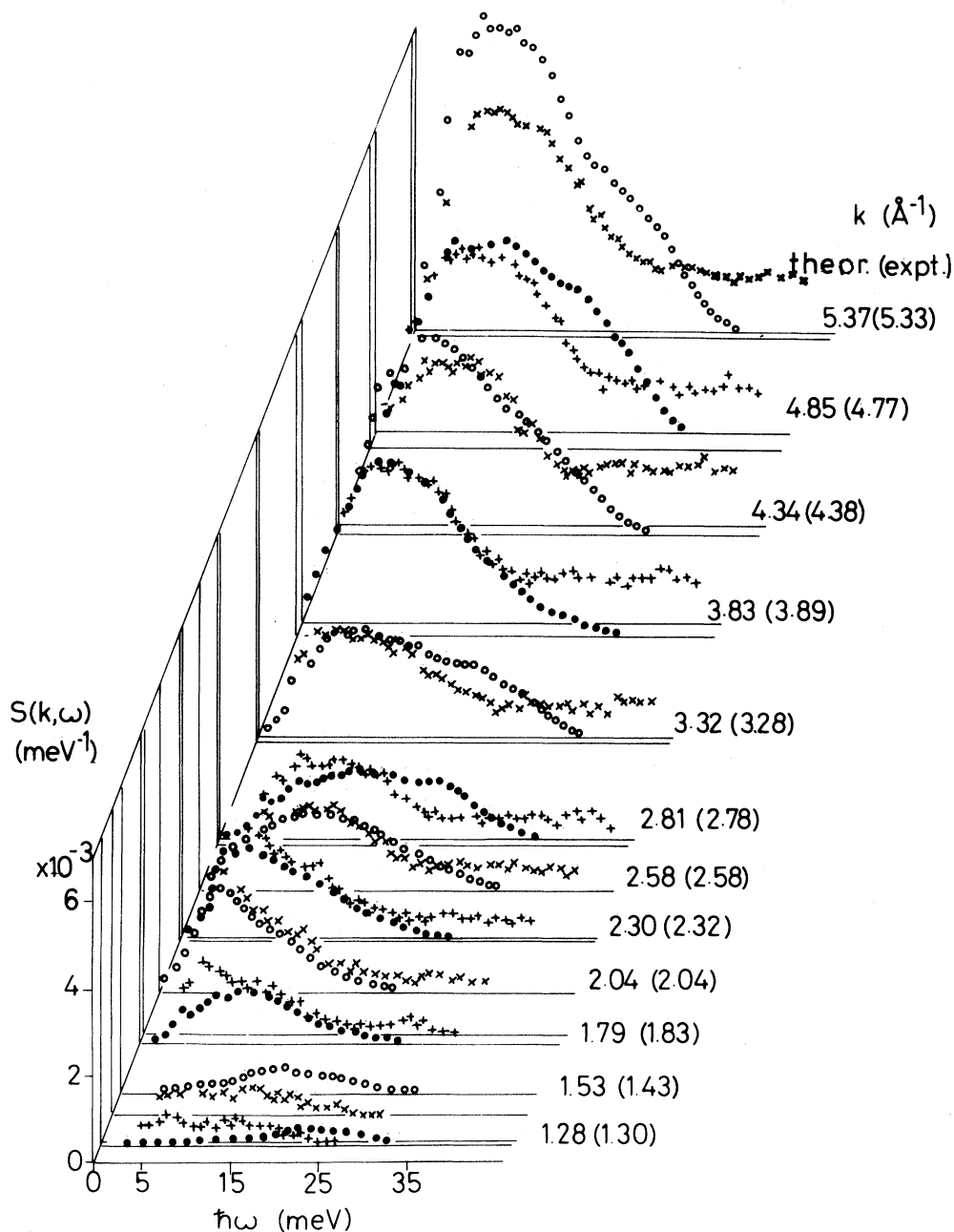


FIG. 15. Dynamical structure factor $S(k, \omega)$ for amorphous $\text{Ca}_{0.70}\text{Mg}_{0.30}$: crosses, experiment; circles, theory (one-phonon part only, $T=6$ K; cf. text).

ing of the low-energy excitations with raising temperature.

2. Dispersion law of propagating collective excitations

It is clearly visible that the peak position in $S(k, \omega)$ shifts to very small frequencies if k is near a peak in the static structure factor. However, it is

very difficult to derive a dispersion law quantitatively. The most direct way would be to use the first and second moments of the dynamical structure factor as a measure for the peak position and the width of the spectrum—unfortunately, this method cannot be applied to the experimental spectra, since the contribution from the hydrogen vibrations cannot be subtracted. The dispersion law plotted in Fig. 17

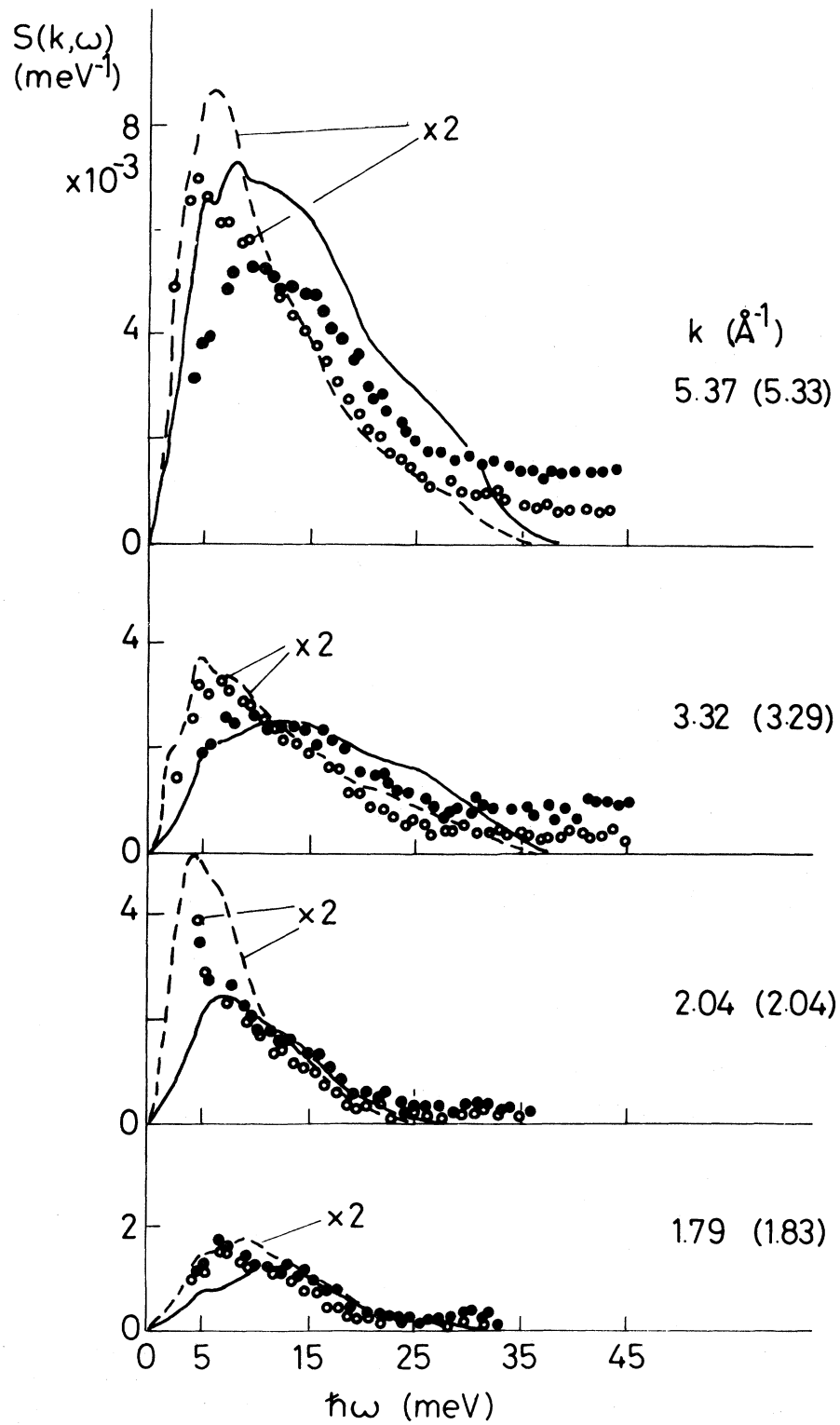


FIG. 16. Temperature dependence of the dynamical structure factor for a few selected constant- k scans. Full line, theory ($T=6$ K); dashed line, theory ($T=273$ K); closed circles, experiment ($T=6$ K); open circles, experiment ($T=273$ K).

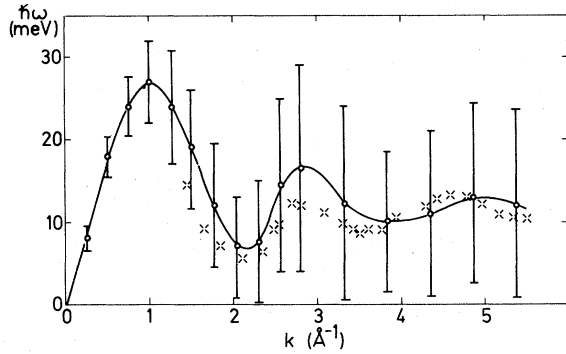


FIG. 17. Dispersion law for propagating collective excitations. The circle indicates the peak in the theoretical $S(k, \omega)$, the bars show the width at half-maximum, and the crosses give the peaks in the observed spectrum (cf. text).

has been derived from the peaks of a smooth interpolation of the measured curves. Compared to the experimental dispersion curves, the theoretical result is shifted to slightly higher frequencies. At larger k values the dispersion is stronger than found in the experiment and the second minimum occurs at higher wave numbers. The minima in the dispersion law at the wave numbers of the peaks in the static structure factor have been explained⁷ as arising from a “diffuse umklapp scattering”—in complete analogy to the polycrystalline case.

3. Generalized frequency spectrum

Experimentally, the vibrational DOS is determined using a technique⁵³ which in principle samples the coherent one-electron scattering cross section over a large region of wave-number space to average out the coherence effects inherent in each individual spectrum. In terms of the dynamical structure factor $S(k, \omega)$, this generalized DOS is given by

$$g'(\omega) \propto \frac{\hbar\omega}{n(\omega)+1} \frac{1}{k_{\max}^4 - k_{\min}^4} \times \int_{k_{\min}}^{k_{\max}} e^{2W(k)} S(k, \omega) k dk. \quad (31)$$

Equation (31) refers to the one-component case. For polyatomic materials, the contributions of the individual components to $S(k, \omega)$ are weighted by the factors b_α as defined by Eq. (29). This means that the incoherent sampling technique measures only a generalized phonon DOS in which the partial contributions are weighted according to their neutron scattering amplitudes and masses. In the case of

Ca-Mg alloys $b_{\text{Mg}}/b_{\text{Ca}}$ is 1.8–1.6 (depending on k and T via the Debye-Waller factor). This means that the incoherent sampling technique overestimates the Mg contribution to the DOS. $g'(\omega)$ has been calculated using Eqs. (28) and (31) [as has been done in the experiment, we have set $e^{2W} = 1$ in Eq. (31)] and agrees reasonably well with $g(\omega)$ (Fig. 10). This justifies the use of this technique for estimating $g(\omega)$. In principle, it is the theoretical $g'(\omega)$ that should be compared with experiment.

E. Elastic and thermodynamic properties

The longitudinal and transverse velocities of sound may be estimated from the slope of the long-wavelength limit of the dispersion relations with the result $V_L = 4.67 \times 10^5 \text{ cm s}^{-1}$ and $V_T = 2.34 \times 10^5 \text{ cm s}^{-1}$. The isothermal bulk modulus B_T of an isotropic solid is given by $B_T = \rho(V_L^2 - \frac{4}{3}V_T^2)$, where ρ is the density. For amorphous Ca_7Mg_3 we get $B_T = 2.29 \times 10^{11} \text{ dyn cm}^{-2}$. This is only 1.3% lower than B_T averaged over the pure crystalline metals, $B_T = 2.32 \times 10^{11} \text{ dyn cm}^{-2}$ [the theoretical bulk moduli for the pure metals are $B_T = 3.40 \times 10^{11} \text{ dyn cm}^{-2}$ (Mg) and $B_T = 1.85 \times 10^{11} \text{ dyn cm}^{-2}$ (Ca), in good agreement with the experimental values⁵⁴ of $B_T = 3.69 \times 10^{11} \text{ dyn cm}^{-2}$ (Mg) and $B_T = 1.69 \times 10^{11} \text{ dyn cm}^{-2}$ (Ca)].

On the other hand, the elastic Debye temperature is given in terms of the sound velocities by

$$\Theta_D = \frac{\hbar\omega_D}{k_B} = \frac{\hbar}{k_B} 2\pi \left[\frac{9n}{4\pi} \right]^{1/3} \left[\frac{1}{V_L^3} + \frac{2}{V_T^3} \right]^{-1/3} \quad (32)$$

and is calculated to be $\Theta_D = 234 \text{ K}$. This is 17% lower than the average $\Theta_D = 282 \text{ K}$ calculated from Θ_D for the pure metals [Θ_D (Ca) = 234 K, Θ_D (Mg) = 390 K (theory); Θ_D (Ca) = 219 K, Θ_D (Mg) = 396 K (theory)]. Both results together suggest that the longitudinal elastic modes are comparable in the glass and in the crystalline mixture, whereas the transverse elastic modes are somewhat softer in the glassy phase.

The high-temperature value $\Theta_D(\infty)$ of the thermodynamic Debye temperature can be calculated from the second frequency moment of the TDOS, $\Theta_D(\infty) = k_B^{-1} (5\langle\omega^2\rangle/3)^{1/2}$ with the result $\Theta_D(\infty) = 270 \text{ K}$.

The same difference between $\Theta_D(0)$ and $\Theta_D(\infty)$ has also been found in the $\Theta_D(T)$ curves calculated from the experimental frequency spectra of Cu-Zr and Mg-Zn glasses⁵ and again suggests that the characteristic softening of phonon modes in the amorphous phase affects primarily the long-

wavelength transverse modes. However, via the diffuse umklapp mechanism, this affects also the dispersion of short-wavelength modes near $k \sim Q_p$.^{7,55}

IV. CONCLUSIONS

We have presented a theoretical investigation of the atomic structure and the vibrational dynamics of the metallic glass $\text{Ca}_{70}\text{Mg}_{30}$. The results of this study have been compared with an earlier inelastic neutron scattering experiment.

The results demonstrate that the microscopic theory of amorphous alloys has now been developed to a point where a quantitative comparison with experiment is possible. The main results may be characterized as follows:

(a) The experiment had shown that the vibrational TDOS of the metallic glass is essentially a broadened version of the TDOS of the corresponding polycrystalline alloy. The present theoretical investigation of the TDOS together with the LDOS and its dependence on the local structural parameters demonstrates that the additional low- and high-energy modes characteristic of the amorphous state are correlated with the existence of "defect" regions in the glasses and that they are probably of a localized character.

(b) The dispersion law for propagating collective excitations in glasses may be explained in terms of a diffuse umklapp scattering—the main peak in the static structure factors acts as a "smeared-out reciprocal-lattice point."

(c) The longitudinal long-wavelength phonons have comparable energies in the glass and in the po-

lycrystal, whereas the transverse modes appear to be considerably softened. Via the diffuse-umklapp-scattering mechanism,^{7,55} the soft long-wavelength transverse phonons are coupled to short-wavelength collective excitations with $k \sim Q_p$.

(d) The reasons for the softening of transverse propagating modes is not immediately clear from the recursion calculation—which, of course, has much of the character of a computer experiment. In this connection, the study of the elastic and plastic properties of metallic glasses via a homogeneous-deformation computer experiment^{41,56,57} are more instructive. They suggest that the absence of crystalline symmetry allows for a more effective relaxation of shear strains by internal displacement which are forbidden in the polycrystal. A detailed study of this question is planned to be presented elsewhere.⁴¹

ACKNOWLEDGMENTS

Part of this work has been performed during a sabbatical visit to the Cavendish Laboratory of the University of Cambridge. The author gratefully acknowledges the award of a fellowship. I am indebted to Professor V. Heine for many stimulating discussions and to Mr. C. Nex for introducing me to the use of the Cambridge Recursion Program Library. I am grateful to Dr. J. B. Suck for many discussions and for sending detailed, partially unpublished information on his experimental results, and to Professor T. Egami and Professor V. Vitek for discussions on atomic-level stresses. Partial financial support has been given by the Fonds zur Förderung der Wissenschaftlichen Forschung in Österreich under Project Nos. 3857 and 4551.

*Permanent address.

¹See, e.g., various contributions in *Ab initio Calculations of Phonon-Dispersion Relations*, edited by J. T. Devreese (Plenum, New York, 1982).

²D. Weaire and P. C. Taylor, in *Dynamical Properties of Solids*, edited by A. A. Maradudin and G. K. Horton (North-Holland, Amsterdam, 1980), Vol. 4.

³J. Hafner, in *Glassy Metals I*, Vol. 46 of *Topics in Applied Physics*, edited by H. Beck and H. J. Güntherodt (Springer, Berlin, 1981), Chap. 6.

⁴J. Hafner, in *Ab initio Calculations of Phonon-Dispersion Relations*, Ref. 1, p. 151.

⁵J. B. Suck and H. J. Rudin, in *Glassy Metals II, Topics in Applied Physics*, edited by H. Beck and H. J. Güntherodt (Springer, Berlin, in press).

⁶S. R. Nagel and A. Rahman, *Phys. Rev. Lett.* **47**, 1665 (1981).

⁷J. Hafner, *J. Phys. C* **14**, L287 (1981).

⁸J. B. Suck, H. Rudin, H. J. Güntherodt, H. Beck, J. Daubert, and W. Gläser, *J. Phys. C* **13**, L167 (1980), and in *Liquid and Amorphous Metals*, NATO-ASI Proceedings, Series E, edited by E. Lüscher and H. Coufal (Sijthoff and Noordhoff, Alpen van Rijn, 1981).

⁹T. M. Holden, J. S. Dugdale, G. C. Hallam, and D. Pavuna, *J. Phys. F* **11**, 1737 (1981).

¹⁰J. B. Suck, H. Rudin, H. J. Güntherodt, and H. Beck, *J. Phys. C* **13**, L1045 (1980).

¹¹J. B. Suck, H. Rudin, H. J. Güntherodt, and H. Beck, *J. Phys. C* **14**, 2305 (1981).

¹²J. B. Suck, H. Rudin, H. J. Güntherodt, and H. Beck, *Proceedings of the IVth International Conference on Rapidly Quenched Metals, Sendai, 1981*, edited by T. Masumoto and K. Suzuki (Japan Institute of Metals, Sendai, 1982), p. 407.

¹³J. B. Suck, H. Rudin, H. J. Güntherodt, and H. Beck, *J. Phys. F* **11**, 1375 (1981).

- ¹⁴J. B. Suck, H. Rudin, H. J. Güntherodt, D. Tomanek, H. Beck, C. Morkel, and W. Gläser, *J. Phys. (Paris) Colloq.* **41**, C8-175 (1980).
- ¹⁵C. G. Windsor, H. Keyrandish, and M. C. Narasimhan, *Phys. Lett.* **70A**, 485 (1979).
- ¹⁶J. J. Rehr and R. Alben, *Phys. Rev. B* **16**, 2400 (1977).
- ¹⁷L. von Heimendahl, *J. Phys. F* **9**, 161 (1979).
- ¹⁸R. Yamamoto, T. Mihara, K. Haga, and M. Doyama, *Solid State Commun.* **36**, 377 (1980).
- ¹⁹R. Yamamoto, K. Haga, T. Mihara, and M. Doyama, *J. Phys. F* **10**, 1389 (1980).
- ²⁰Y. Ishii and T. Fujiwara, *J. Phys. F* **10**, 2125 (1980).
- ²¹S. Kobayashi and S. Takeuchi, *J. Phys. C* **13**, L969 (1980).
- ²²J. Hafner, *Z. Phys. B* **22**, 351 (1975); **24**, 351 (1976).
- ²³J. Hafner and H. Eschrig, *Phys. Status Solidi B* **72**, 179 (1975).
- ²⁴J. Hafner, *J. Phys. F* **6**, 1243 (1976).
- ²⁵J. Hafner, *Phys. Rev. B* **15**, 617 (1977); **19**, 5094 (1979).
- ²⁶J. Hafner, *Phys. Rev. A* **16**, 351 (1977).
- ²⁷J. Hafner, *Phys. Rev. B* **21**, 406 (1980).
- ²⁸J. Hafner and L. von Heimendahl, *Phys. Rev. Lett.* **42**, 386 (1979).
- ²⁹T. Mizoguchi, N. Shiotani, U. Mizutani, T. Kudo, and S. Yamada, *J. Phys. (Paris) Colloq.* **41**, C8-183 (1980).
- ³⁰L. von Heimendahl, *Phys. Status Solidi B* **86**, 549 (1978).
- ³¹For a general discussion of the equation-of-motion method as applied to electronic and vibrational problems, see, e.g., D. Beemann and R. Alben, *Adv. Phys.* **26**, 339 (1977).
- ³²The recursion technique has recently been reviewed in a series of papers by V. Heine, R. Haydock, D. Bulletin, and M. J. Kelly, in *Solid State Physics*, edited by H. Ehrenreich, D. Turnbull, and F. Seitz (Academic, New York, 1981), Vol. 35. The first application of this technique to phonons in amorphous materials has been made by P. Meek, *Philos. Mag.* **33**, 897 (1976). Some of the routines used in this work are based on Meek's programs which have been obtained from the Cambridge Recursion Program Library.
- ³³C. M. M. Nex, *J. Phys. A* **11**, 653 (1978).
- ³⁴M. W. Finnis, *J. Phys. F* **4**, 1645 (1974).
- ³⁵For a more detailed discussion of the influence of electronic many-body effects on metallic interatomic potentials see, e.g., G. Jacucci and R. Taylor, *J. Phys. F* **11**, 787 (1981), and J. Hafner, in *Proceedings of the Spring College on Amorphous Solid and the Liquid State, International Centre for Theoretical Physics, Trieste, 1982* (unpublished).
- ³⁶J. Hafner, *Phys. Rev. B* **10**, 4151 (1974).
- ³⁷For an investigation of the volume effect on the pair potential, see, J. Hafner, *J. Phys. F* **5**, 1439 (1975).
- ³⁸The author is indebted to Dr. von Heimendahl for sending his relaxation program.
- ³⁹J. R. Finney, *Proc. R. Soc. London Ser. A* **319**, 479 (1970).
- ⁴⁰H. Rudin (private communication).
- ⁴¹J. Hafner (unpublished).
- ⁴²J. F. Sadoc and M. Dixmier, *Mater. Sci. Eng.* **23**, 187 (1976).
- ⁴³J. M. Cowley, *J. Appl. Phys.* **21**, 24 (1950).
- ⁴⁴G. S. Cargill III and F. Spaepen, *J. Non-Cryst. Solids* **43**, 91 (1981).
- ⁴⁵J. L. Finney and J. Wallace, *J. Non-Cryst. Solids* **43**, 165 (1981).
- ⁴⁶P. Jacobaeus, J. V. Madsen, F. Kragh, and R. M. J. Cotterhill, *Philos. Mag. B* **41**, 11 (1980); J. Hafner, *J. Phys. F* **12**, L205 (1982).
- ⁴⁷T. Egami, K. Maeda, and V. Vitek, *Philos. Mag. A* **41**, 883 (1980); D. Srolovitz, K. Maeda, S. Takeuchi, T. Egami, and V. Vitek, *ibid.* **44**, 847 (1981).
- ⁴⁸D. Srolovitz, T. Egami, and V. Vitek, *Phys. Rev. B* **24**, 6936 (1981).
- ⁴⁹K. Huang, *Proc. R. Soc. London Ser. A* **203**, 178 (1950).
- ⁵⁰D. Srolovitz, T. Egami, V. Vitek, and J. Hafner (unpublished).
- ⁵¹J. Hafner (unpublished).
- ⁵²F. Gompf, *Workshop: Order in Disordered Materials, Bad Honnef, 1982* (unpublished).
- ⁵³V. S. Oskotskii, *Fiz. Tverd. Tela Leningrad* **9**, 550 (1967) [*Sov. Phys.—Solid State* **9**, 420 (1967)]; M. M. Bredov, B. A. Kotov, N. M. Okumeva, V. S. Oskotskii, and A. L. Shakh-Budagov, *ibid.* **9**, 287 (1967) [*ibid.* **9**, 214 (1967)].
- ⁵⁴K. A. Gschneider, in *Solid State Physics*, edited by H. Ehrenreich, F. Seitz, and D. Turnbull (Academic, New York, 1964), Vol. 16.
- ⁵⁵J. Hafner, in *Proceedings of the IV International Conference on Rapidly Quenched Metals, Sendai, 1981*, edited by T. Masumoto and K. Suzuki (Japan Institute of Metals, Sendai, 1982), p. 411.
- ⁵⁶D. Weaire, M. F. Ashby, J. Logan, and M. J. Weins, *Acta Metall.* **19**, 779 (1971).
- ⁵⁷M. Doyama, R. Yamamoto, and H. Matsuoka, in *Proceedings of the IV International Conference on Rapidly Quenched Metals, Sendai, 1981*, edited by T. Masumoto and K. Suzuki (Japan Institute of Metals, Sendai, 1982), p. 233; V. Vitek, D. Srolovitz, and T. Egami, *ibid.* p. 241.